

Searching for Mixed Octahedral-Tetrahedral Interstitial Hydrogen Occupation

in Pd-Ti Sublattices:

A Computational Study

Isaac Metcalf

Department of Materials Science and Engineering

Signature of Author:

Certified by: Yet-Ming Chiang, Kyocera Professor, MIT Department of Materials
Science & Engineering

Accepted By: Juejun Hu, Associate Professor of Materials Science and Engineering,
Chair, DMSE Undergraduate Committee

Abstract

With hydrogen conversion and storage technologies promising a revolution in the energy industry if volumetric energy density is increased, the loading of hydrogen to high concentrations in metal lattices has become of special interest. Here we use Projector Augmented-wave density functional theory methods to search the Pd-Ti-H system for stable instances of mixed tetrahedral-octahedral site occupation. We compute the energies of 42 hydrides constructed from seven metal sublattices: Ni₃Ti-prototype Pd₃Ti, CdI₂-prototype PdTi₂, and FCC four-atom unit cells of Pd, Pd₃Ti, PdTi, PdTi₃, and Ti. Our results suggest that mixed octahedral-tetrahedral occupation is energetically unfavorable in most cases, but a Li₃Bi-prototype hydride may be stable within the Pd_{1-x}Ti_xH₃ system.

Table of Contents

<u>Introduction</u>	4
<u>Methods</u>	7
i. A brief overview of Density Functional Theory	7
ii. Atomic Simulation Environment (ASE)	12
iii. The Projector Augmented-Wave (PAW) method	13
iv. Algorithm	15
<u>Experiments</u>	17
i. Relevant structures in the Pd-Ti binary phase diagram	18
ii. FCC Pd-Ti Solid Solutions	23
iii. Phase Diagram	25
<u>Results and Discussion</u>	26
i. PdTi ₂	26
ii. Pd ₃ Ti	28
iii. FCC Pd-Ti Solid Solutions	29
iv. Phase Diagram	31
<u>Conclusion</u>	34
<u>Works Cited</u>	35
<u>Appendices</u>	36
Appendix A	36
Appendix B	39
Appendix C	44

Introduction

Palladium hydride (PdH_{1-x}) is the prototypical metal-hydrogen phase; first observed in the 1860s, PdH_{1-x} has since remained the most academically interesting of all metal hydrides. The special interest in and intriguing properties of PdH_{1-x} stem partially from the fact that it is not a true hydride (for which hydrogen would be an anion), but instead a solid solution of metallic hydrogen in palladium. Hydrogen atoms occupy octahedral sites in the palladium FCC lattice (fig. 1a) up to a Pd:H ratio of 1:1, forming a rock-salt structure (fig. 2b).

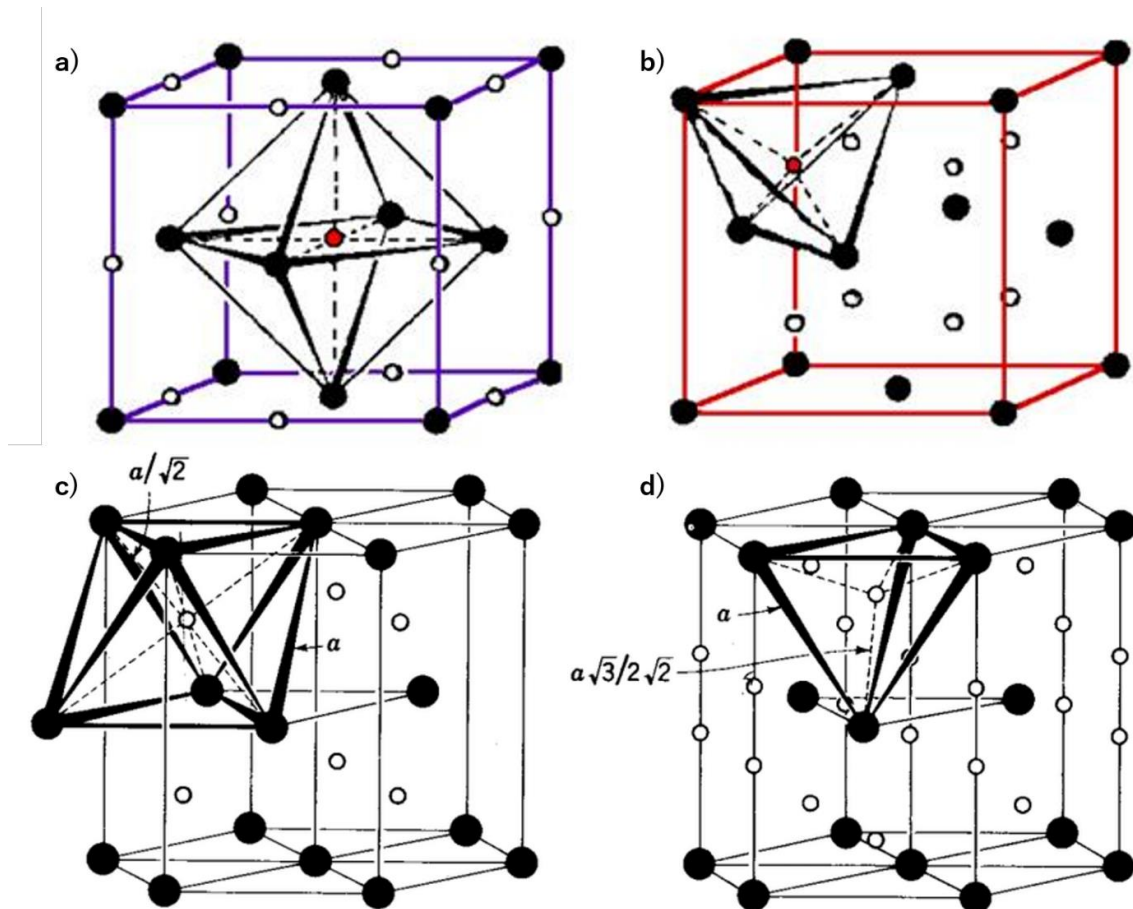


Figure 1: (a) An octahedral, and (b) a tetrahedral site in an FCC unit cell. (c) An octahedral, and (d) a tetrahedral site in an HCP unit cell. There are two tetrahedral sites and one octahedral site per lattice point in both lattices.

Palladium is by no means the only metal which accepts hydrogen; indeed, nearly all metals will form binary M-H compounds, although these are usually of an ionic character.

Titanium, for example, forms the semi-ionic hydride TiH_{2-x} . Titanium hydride exhibits several phase transitions as hydrogen loading is increased. For low hydrogen concentrations, TiH_{2-x} retains the HCP structure of pure titanium. As [H] increases a fluorite phase begins to emerge (fig. 2d), with H occupying the tetrahedral sites of an FCC Ti lattice (fig 1b). Near stoichiometry TiH_2 adopts a distorted, body-centered tetragonal structure, which is unstable unless it remains under hydrogen atmosphere.

Besides the rock-salt and fluorite structures, other options for interstitial occupation include zincblende, in which every other tetrahedral site is occupied, the Li_3Bi prototype (also formed by LaH_3), in which all tetrahedral and octahedral sites are occupied, and the AgAsMg -prototype, in which zincblende sites and octahedral sites are occupied. In a hexagonal sublattice, hydrogen might occupy octahedral sites (NiAs), alternating tetrahedral sites (wurtzite), both octahedral and wurtzite sites, tetrahedral sites, or both octahedral and tetrahedral sites. The last three structures are unlikely to be stable, since nearest-neighbor hexagonal tetrahedral sites share faces and therefore there would be little screening between hydrogen nuclei.

Given that PdH exhibits octahedral occupation of hydrogen, and TiH_2 tetrahedral occupation, it is possible that mixed tetrahedral-octahedral occupation may occur within PdH - TiH_2 alloys. The Li_3Bi structure might become stable at high hydrogen pressure.

Alternately, some (Pd,Ti) lattice might accept H interstitially in an AgAsMg-prototype configuration. This thesis will use density functional theory (DFT) methods to search for stable instances of mixed occupation within the Pd-Ti-H ternary phase diagram.

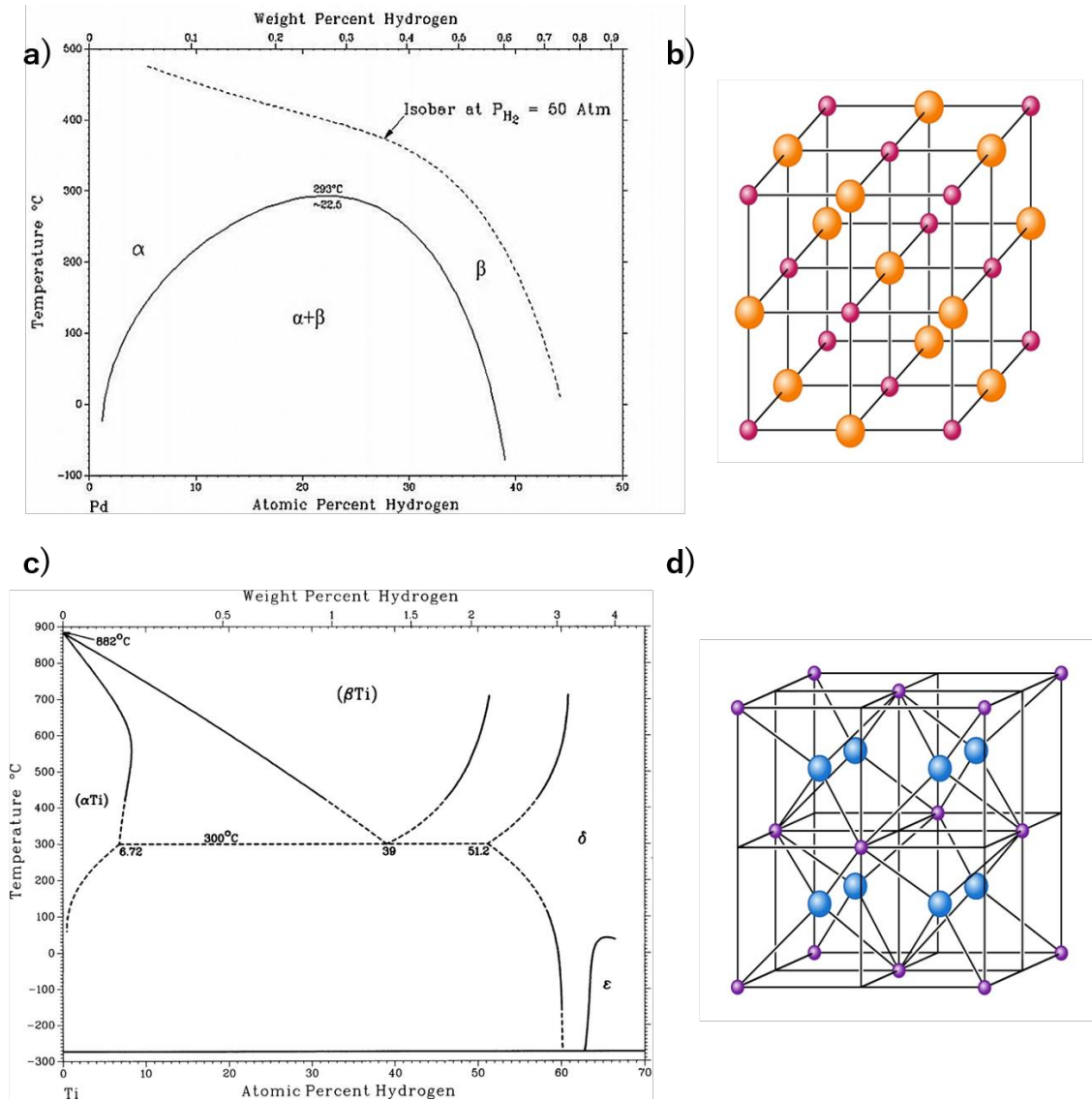


Figure 2: (a) The Pd-H binary phase diagram, reproduced from [1]. (b) The halite structure of the α phase of PdH_{1-x} . Hydrogen atoms occupy the octahedral interstitial sites within an FCC Pd lattice. (c) The Ti-H binary phase diagram, reproduced from [2]. (d) The fluorite structure of the δ phase of TiH_{2-x} . Hydrogen atoms occupy the tetrahedral interstices within an FCC Ti Lattice.

Methods

i. A brief overview of density functional theory

Density functional theory has emerged in the last 30 years as an immensely useful tool for the prediction of molecular structure and properties. In general, DFT finds its use in the treatment of many-body quantum systems. For problems in which DFT is relevant, the system is a collection of electrons and nuclei - for example, the unit cell of a crystal, or a molecule in a gas. A many-body wavefunction ψ then defines the position of each electron and nucleus in space.

Most quantum chemistry methods begin by invoking the Born-Oppenheimer approximation, which argues that the large difference in mass between an electron and a nucleus gives the two particles drastically different time scales of motion, such that nuclear kinetic energies can be neglected and nuclear positions can enter the Hamiltonian parametrically. Using the Born-Oppenheimer approximation, the electrons in the system can be treated as moving in a fixed potential field generated by the nuclei. The Schrodinger equation of a system of N electrons is then rewritten as

$$\left[-\frac{\hbar^2}{2m} \sum_{i=1}^N \nabla_i^2 + \sum_{i=1}^N V_{ext}(r_i) + \sum_{i=1}^N \sum_{j<i}^N U(r_i, r_j) \right] \psi = E\psi \quad (1)$$

where r_i is the position of the i^{th} electron. From left to right, the left-hand-side terms give the total electron kinetic energy T , the electron energy from the nuclear potential field $V_{ext}(r)$ and the electron-electron interaction energy $U_{el}(u, v)$. Solving this equation gives

an “adiabatic potential energy surface”, $E(R_1, R_2, \dots, R_M)$, which is a function of the locations of the M nuclei in the system. Finding the lowest-energy eigenstate ψ_{GS} and eigenvalue E_{GS} of this equation and minimizing E_{GS} with respect to nuclear positions gives the (nearly) exact ground-state configuration of the N -electron, M -nucleus system.

In practice, such a direct approach is intractable except for trivially simple problems. Each electron has three spatial degrees of freedom, giving $3N$ total degrees of freedom for the electronic component of the system alone. For most molecules and solids of interest for DFT, the Schrodinger equation is a many-body problem with several hundred to several thousand dimensions. The solution to such an equation is far beyond the capabilities of any present computer.

The utility of DFT lies in its ability to find approximate numerical solutions to such many-body quantum systems efficiently. In other words, DFT can simulate the structure and behavior of molecules and solids. Predictions from DFT can be used to inform physical experiments, or to discern the cause of observed chemical phenomena. In both cases, the use of DFT allows for a greater understanding of the system under observation with far fewer experiments.

DFT hinges on a proof by P. Hohenberg and W. Kohn [3], given in 1964, that the position of electrons as defined by a wavefunction ψ has the same physical significance as the density of the electron probability cloud, $n(r) \equiv \sum_{i=1}^N |\psi_i(r)|^2$, where $\psi_i(r)$ is the

wavefunction of the i^{th} electron. Importantly, the electron density is a function of only three spatial coordinates rather than $3N$; solving for an energy-minimizing electron density, then, would seem a much more tractable problem than searching for a ground state electron configuration. The first of the *Hohenberg-Kohn theorems* states that the ground-state energy of a many-particle system is a unique functional of electron density. That is, given a set of N interacting electrons in an external potential $V_{ext}(r)$, there is a one-to-one correspondence between E_0 and $n(r)$. The second Hohenberg-Kohn theorem shows that we can construct an energy functional $E[n(r)]$ which can be minimized over $n(r)$ to obtain the true ground-state energy $E_0 = E[n_0(r)]$, with $n_0(r)$ the electron density of the ground state.

The Hohenberg-Kohn theorems prove that a many-particle quantum system can be described uniquely by its electron probability density, and that the ground state of such a system can be found by minimizing an energy functional with respect to this density.

However, these results say nothing about how to construct an energy functional and perform useful calculations. For this we require the Kohn-Sham equations [4], a set of non-physical equations which re-imagines the true electron density $n(r)$ as the sum of density contributions from N fictitious non-interacting electron wavefunctions ϕ_i within some effective potential called the Kohn-Sham potential, V_{KS} , such that

$$\left[\frac{\hbar^2}{2m} \nabla^2 + V_{KS}(r) \right] \phi_i(r) = \epsilon_i \phi_i(r). \quad (2)$$

In general, neither the ϕ_i 's nor the ϵ_i 's above have any physical significance. However, the

amplitude squared of the Slater determinant of the N lowest-energy solutions ϕ_i to this *Kohn-Sham equation* gives $n(r)$, and the sum of the N lowest ϵ_i 's gives E_0 . Comparing this equation with eqn 1, we see that we've circumvented the many-body complications of this problem, greatly simplifying the Hamiltonian, by wrapping all many-body effects into the Kohn-Sham potential. The trade-off is that V_{KS} is unknown, but fortunately it can be approximated.

Kohn and Sham showed that V_{KS} could be expanded to give

$$V_{KS}(r) = V_{ext}(r) + \frac{e^2}{2} \int \frac{n(r')}{|r-r'|} dr' + V_{XC}(r), \quad (3)$$

where $V_{ext}(r)$ is the nuclear potential field, $\frac{e^2}{2} \int \frac{n(r')}{|r-r'|} dr'$ is the Coulomb field created by the electron density, and $V_{XC}(r)$ is the so-called "exchange-correlation potential." Every term in V_{KS} is known besides V_{XC} , which holds the effects of exchange (which gives rise to the repulsive force of the Pauli exclusion principle) and correlation (the quantum effect by which the state of one particle can affect the state of another). Most attempts to quantify V_{XC} begin with a local density approximation (LDA), which treats $V_{XC}(r)$ as the corresponding known potential of a uniform electron gas $V_{XC}^{e-gas}[n(r)]$, where $n(r)$ is the electron density at the point r :

$$V_{XC}(r) \approx V_{XC}^{LDA}(r) = V_{XC}^{e-gas}[n(r)]. \quad (4)$$

As one might expect, V_{XC}^{LDA} is often a poor approximation to the true V_{XC} . The generalized gradient approximation (GGA) takes a slightly more nuanced approach, incorporating the

local gradient of electron density as a so called “enhancement factor”, $F_{XC}[n(r), \nabla n(r)]$:

$$V_{XC}^{GGA}(r) = V_{XC}^{e-gas}[n(r)] F_{XC}[n(r), \nabla n(r)]. \quad (5)$$

Here F_{XC} is some unspecified functional which depends somehow on both $n(r)$ and its gradient. The enhancement factor can differ based on the DFT algorithm in use, and different F_{XC} ’s perform better in different systems.

With the Kohn-Sham equations in hand, an algorithmic approach to solving a problem with DFT can be envisioned. The goal of a DFT calculation is to converge on a ground-state electron density $n(r)$ which solves the Kohn-Sham equations. From $n(r)$, the electronic configuration and energy of the system can be found. The skeleton of an algorithm, as outlined in [5], is as follows:

1. Define a trial electron density $n_{test}(r)$ and use it to approximate V_{KS} , using some approximate V_{XC} . We obtain $n_{test}(r)$ with a single-Slater-determinant “reference wavefunction,” usually having the symmetry properties of the system. For solids, the Slater determinant is formed from a basis set of plane waves.
2. Using V_{KS} , find the N lowest-energy single-particle wavefunctions ϕ_i from the Kohn-Sham equations.
3. Using $n(r) = \sum |\phi_i(r)|^2$, find the electron density n_{KS} corresponding to the ϕ_i .
4. If $n_{KS}(r) = n_{test}(r)$ to within the tolerances of the computation (that is, if n_{test} is self-consistent), $n_{test}(r)$ is the ground state electron density. If not, update n_{test} using

the results of the computation.

How exactly to go about updating n_{test} in step 4 is a problem for the writer of the DFT algorithm, but the problem isn't meaningfully different from that of other algorithms which search for self-consistency.

ii. Atomic Simulation Environment (ASE)

Calculations for this thesis were performed through ASE [6], a free python-based atomic simulation environment. ASE itself doesn't perform DFT calculations; rather, it offers a platform to configure atomic environments, and exports calculations to one of the several "calculators" compatible with the platform.

ASE lets the user create an atomic environment through "Atoms" objects, which define the atomic numbers and positions of a collection of atoms in a simulation. Properties of each element (mass, radius, etc.) are stored within ASE's "data module." Atoms can be placed within a unit cell using the "Cell" object, which defines the lengths and angles of the simulated crystal's lattice vectors. A unit cell can be varied and rescaled between measurements to minimize energy with respect to lattice parameters. Once an input unit cell is defined, ASE can use a "Calculator" object to find the energy of the system, which allows the user to optimize structures and compare relative stability of phases. ASE can be used as a platform for practically any quantum chemistry simulation, and is commonly used to

calculate phase diagrams and band structures and to perform nudged elastic band and molecular dynamics simulations.

iii. The Projector Augmented-Wave (PAW) method

The calculator used for simulations in this thesis was GPAW, which uses the projector augmented-wave (PAW) method [7]. PAW is a generalized pseudopotential approach which was created to circumvent the issues encountered by DFT in regions near atomic nuclei. The contribution of core-shell electron wavefunctions near nuclei give the Kohn-Sham potential sharp features which makes the convergence of DFT simulations difficult. Since core-shell electrons are strongly localized, each nuclear potential can be replaced with an effective “pseudopotential” that accounts for both the nucleus and core-shell electrons, and solving the Kohn-Sham equations only for the valence electrons. Taking the “frozen core” approximation, we can estimate an atom’s pseudopotential as system-independent, such that it can be tabulated in advance for every element. However, the loss of information near nuclei can reduce the accuracy of DFT calculations using pseudopotentials.

The PAW method formalizes the pseudopotential approach to smooth the wavefunction without loss of core-electron information. It begins by imagining a linear transformation operator T which takes the (not yet defined) pseudopotential wavefunction $|\tilde{\psi}\rangle$ to the all-electron single-particle wavefunction $|\psi\rangle$ that enters the Kohn-Sham equation:

$$|\psi\rangle = T |\tilde{\psi}\rangle. \quad (6)$$

Once again, $|\psi\rangle$ is the slater determinant of the N single electron wavefunctions $|\phi_i\rangle$ which appear as solutions to equation 2. T need only act near the nuclei, and in smooth regions

$|\tilde{\psi}\rangle$ can be set equal to $|\psi\rangle$. We can then write T as

$$T = 1 + \sum_{a=1}^M T^a \quad (7)$$

Where T^a is localized on the a^{th} nucleus, and the sum runs over all M nuclei in the system.

We call the region in which T^a acts the “augmentation sphere,” and we can expand the pseudo-wavefunction $|\tilde{\psi}^a\rangle$ in each sphere as a linear combination of orthogonal one-electron pseudo-wavefunctions (also not yet defined):

$$|\tilde{\psi}^a\rangle = \sum_{i=1}^N c_i |\tilde{\phi}_i^a\rangle. \quad (8)$$

Since we made $|\tilde{\phi}_i^a\rangle$ orthogonal and we made T linear, the coefficients c_i^a are guaranteed to be the inner products of $|\tilde{\psi}^a\rangle$ with some set of “projection waves” $|p_i^a\rangle$:

$$\langle p_i^a | \tilde{\phi}_j^a \rangle = \delta_{ij} \rightarrow c_i^a = \langle p_i^a | \tilde{\psi}^a \rangle \quad (9)$$

With some manipulation, we can use the above expressions to rewrite T^a as

$$T^a = 1 + \sum_{i=1}^N (|\phi_i^a\rangle - |\tilde{\phi}_i^a\rangle) \langle p_i^a |, \quad (10)$$

and combining the i^{th} $|\tilde{\phi}_i^a\rangle$ from each of the M augmentation spheres into one single-electron wavefunction $|\tilde{\phi}_i\rangle$, we can write

$$T = 1 + \sum_{i=1}^N (|\phi_i\rangle - |\tilde{\phi}_i\rangle) \langle p_i|. \quad (11)$$

What we've gained from this new picture of pseudopotentials is the ability to go back and forth between rough “true” one-electron wavefunctions and smooth one-electron pseudo-wavefunctions. We can now choose the pseudopotential by defining a set of projection waves within the augmentation spheres, hence the name “projector augmented-wave”.

The GPAW calculator [8] uses the PAW method and assumes the frozen-core approximation holds. The $\langle p_i^Z |$ projection waves for each atomic number Z have been tabulated in advance, making GPAW both accurate and efficient for a variety of systems.

iv. Algorithm

This paper compares the relative stability of various Pd-Ti-H phases to predict which are physically realizable. We estimate stability by calculating the potential energy per atom of a bulk phase, and we then compare the energy of phases with the same composition to find the lowest-energy state.

We demonstrate our algorithm on a PdH FCC unit cell. To actually calculate the stability of a phase using the GPAW calculator on ASE, we first import the “Atoms” object and the “GPAW” calculator, and specify that GPAW use a set of plane wave basis states to build its Kohn-Sham one-electron wavefunctions.

```
from ase import Atoms
from gpaw import GPAW, PW
```

GPAW calculates energy by integrating over reciprocal space, which it does by discretizing reciprocal space into a 3D grid of evenly-spaced “k-points.” We set the number of k-points before the calculation. In general the smallest number of k-points is chosen such that the calculated energy is within 0.1eV of the energy with additional k-points. For these calculations, we use $k=6$.

```
k = 6
calc = GPAW(mode=PW(300), kpts=(k, k, k))
```

We then define the positions and atomic numbers of each atom in our unit cell, assuming a lattice constant around 4. This information is stored in an “Atoms” object, along with our calculator and our boundary conditions.

```
a = 4
unitcell=[[a/2,a/2,0],[a/2,0,a/2],[0,a/2,a/2]]
xtal=Atoms('PdH', positions=[[0,0,0],[a/2,a/2,a/2]],
           cell=unitcell, pbc=True, calculator=calc)
```

We can vary the lattice constant parametrically to minimize the energy with respect to ‘a’.

```
energy=[]
for i in range(5):
    x=.9+.05*i
    xtal.set_cell(unitcell*x, scale_atoms=True)
    energy.append(xtal.get_potential_energy())
```

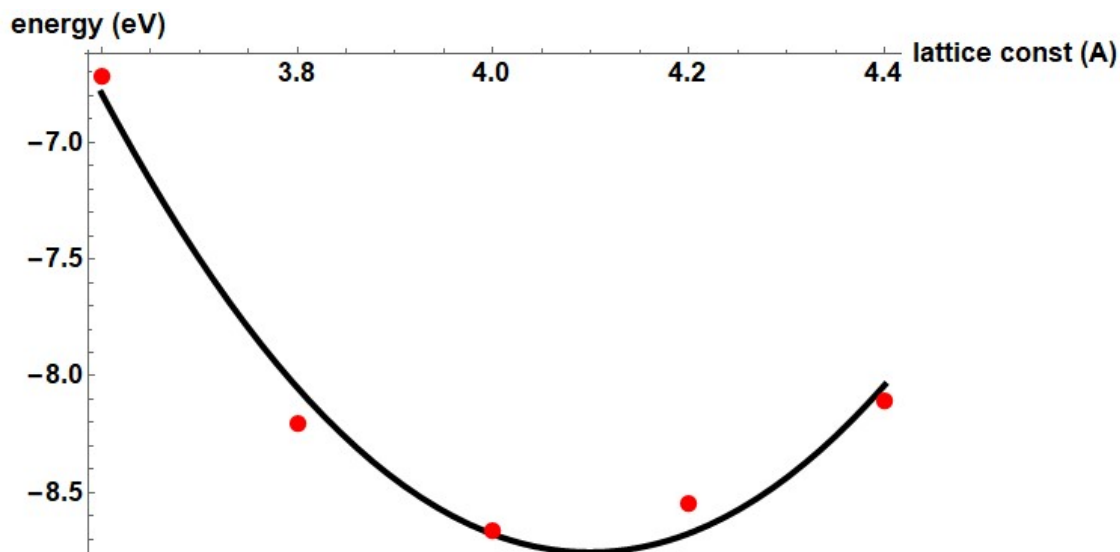


Figure 3: The result of an example computation, of PdH energy as a function of lattice constant. The five computed points (red) are fitted to a quadratic polynomial (black). The minimum of the fit is taken to be the true lattice constant and ground-state energy.

The minimum energy is taken as the energy of the phase, and this energy can be compared to that of other phases with the same composition to judge relative stability. To directly compare stability between structures of different hydrogen concentration, we must account for the free energy of gaseous H_2 , which is a function of hydrogen partial pressure. In general, as the partial pressure of H_2 increases absorption into a solid phase becomes more favorable.

Experiments

Even with density functional theory, fully mapping the ternary Pd-Ti-H phase diagram would be too computationally intensive. If the positions of titanium, palladium, and hydrogen nuclei are taken as free variables, we would have to search over all possible unit cells for any given composition to find the minimum-energy configuration. Instead, the

approach taken here will be to investigate the hydrogen occupancy of a few candidate Pd-Ti sublattices which are *likely* to be stable. Specifically, two categories of sublattices will be examined: relevant stable structures in the Pd-Ti binary phase diagram, and FCC prototype Pd-Ti sublattices. In each case, hydrogen will be placed at interstitial sites in the unit cell, and ground-state energy will be calculated.

i. Relevant structures in the Pd-Ti binary phase diagram

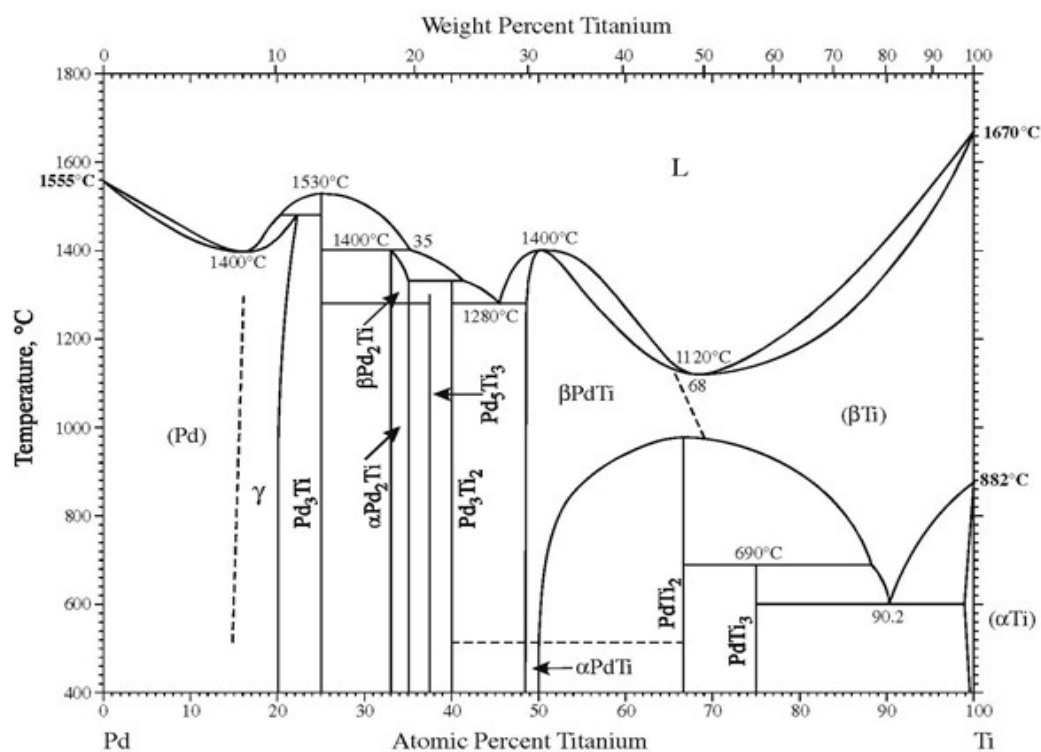
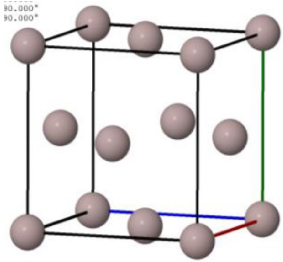
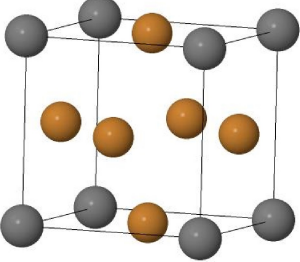


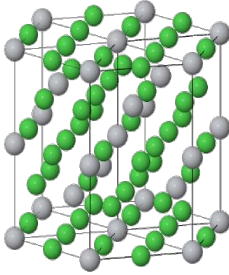
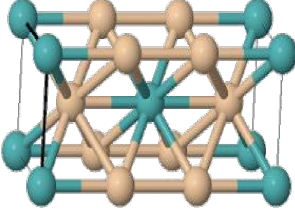


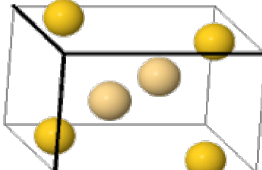
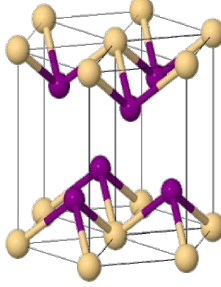
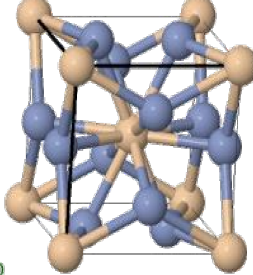
Figure 4: The Palladium-Titanium phase diagram, reproduced from [9]

Moving across the Pd,Ti phase diagram near room temperature, one encounters ten phases: pure FCC palladium, pure HCP titanium, and eight intermediate compounds. The structure of each of these phases is given in table 1, reproduced here from [10]. A reasonable

place to begin the search for structures exhibiting mixed occupancy is to load each of the crystals in this binary phase diagram with hydrogen and observe which interstitial sites are preferentially occupied. The implicit assumption underlying this experiment is that hydrogen will incorporate into the interstices of the Pd,Ti lattice without a phase change. We can see immediately that this assumption is flawed from the Pd-Ti phase diagram, which has a phase change from a hexagonal to a cubic unit cell as the composition of hydrogen is increased. Nevertheless, it gives us a jumping-off point for an otherwise intractable problem.

Constraining our search to phases that share FCC's octahedral and tetrahedral interstitial geometries, three phases from table 1 distinguish themselves: The cubic γ phase, the hexagonal Pd₃Ti phase, and the hexagonal PdTi₂ phase.

Phase	Composition (at% Ti)	Pearson symbol/ Prototype	Illustration
(Pd)	0-15	cF4/Cu (FCC)	
γ	15-22.5	cP4/AuCu ₃	

Pd_3Ti	25	$\text{hP16}/\text{Ni}_3\text{Ti}$	
$\alpha\text{Pd}_2\text{Ti}$	33-35	$\text{tI6}/\text{MoSi}_2$	
Pd_5Ti_3	37.5	$\text{tI8}/\sim$	
Pd_3Ti_2	40	$\text{oC20}/\sim$	
αPdTi	48.5-50	$\text{oP4}/\text{AuCd}$	
PdTi_2	66.7	$\text{hP3}/\text{CdI}_2$	
PdTi_3	75	$\text{cP8}/\text{Cr}_3\text{Si}$	

α Ti	99-100	hP2/Mg (HCP)	
-------------	--------	--------------	---

Table 1: The room-temperature phases of the Pd-Ti phase diagram. Images are from [10]

1. The γ phase

The γ phase of the Pd-Ti system, $\text{Pd}_3\text{Ti}_{1-x}$, has an AuCu_3 prototype. Ti atoms occupy some of the corners of an FCC unit cell, with Pd atoms occupying the face centers. With Ti at every corner the unit cell would have a chemical formula Pd_3Ti , although the phase becomes thermodynamically unfavorable before this concentration. The unit cell of γ - Pd_3Ti is shown in fig. 4, and the positions of the four atoms, four octahedral interstitial sites, and eight tetrahedral interstitial sites are listed in appendix A. While finite computational resources prevented an analysis of the off-stoichiometry $\text{Pd}_3\text{Ti}_{1-x}$ phase, FCC Pd_3Ti was examined as one of the five “solid solution” structures.

2. Pd_3Ti

The Pd_3Ti phase on the Pd-Ti phase diagram adopts a Ni_3Ti prototype. This structure has a 16-atom unit cell, which arrange themselves in a hexagonal configuration. Crystal energy was tested with six different hydrogen interstitial occupations: With no hydrogen (Pd_3Ti), with octahedral sites or wurtzite sites occupied (Pd_3TiH_4), with both octahedral sites and wurtzite sites, or with tetrahedral sites, occupied (Pd_3TiH_8), and with both octahedral sites and

tetrahedral sites occupied ($\text{Pd}_3\text{TiH}_{12}$). The positions of the 16 atoms, the 16 octahedral interstitial sites, the 16 wurtzite sites, and the 32 tetrahedral interstitial sites of Pd_3Ti are listed in appendix A.

3. PdTi_2

PdTi_2 is another hexagonal phase on the Pd-Ti phase diagram. It has the prototype of CdI_2 , such that Ti atoms form an HCP sublattice with Pd atoms occupying alternating layers of octahedral sites. The other half of octahedral sites and all tetrahedral sites are available for hydrogen atoms to fill. Crystal energy was tested with six different hydrogen interstitial occupations: With no hydrogen (PdTi_2), with octahedral site occupied (PdTi_2H), with wurtzite sites occupied (PdTi_2H_2), with both octahedral site and wurtzite sites (PdTi_2H_3), with tetrahedral sites (PdTi_2H_4), and with both octahedral site and tetrahedral sites (PdTi_2H_5). The positions of the three metal atoms, one octahedral site, two wurtzite sites, and four tetrahedral sites are listed in appendix A.

It is unlikely that hexagonal structures with mixed occupation or with full tetrahedral occupation will be stable, due to the proximity and poor screening between occupied interstitial sites. The likelihood of stability diminishes if hydrogen adopts an ionic character in the lattice, as it should as the ratio of titanium to palladium is increased. Nevertheless, a stable instance of such a structure cannot be ruled out completely and would be very interesting if predicted, so these improbable phases are examined along with the more

common prototypes.

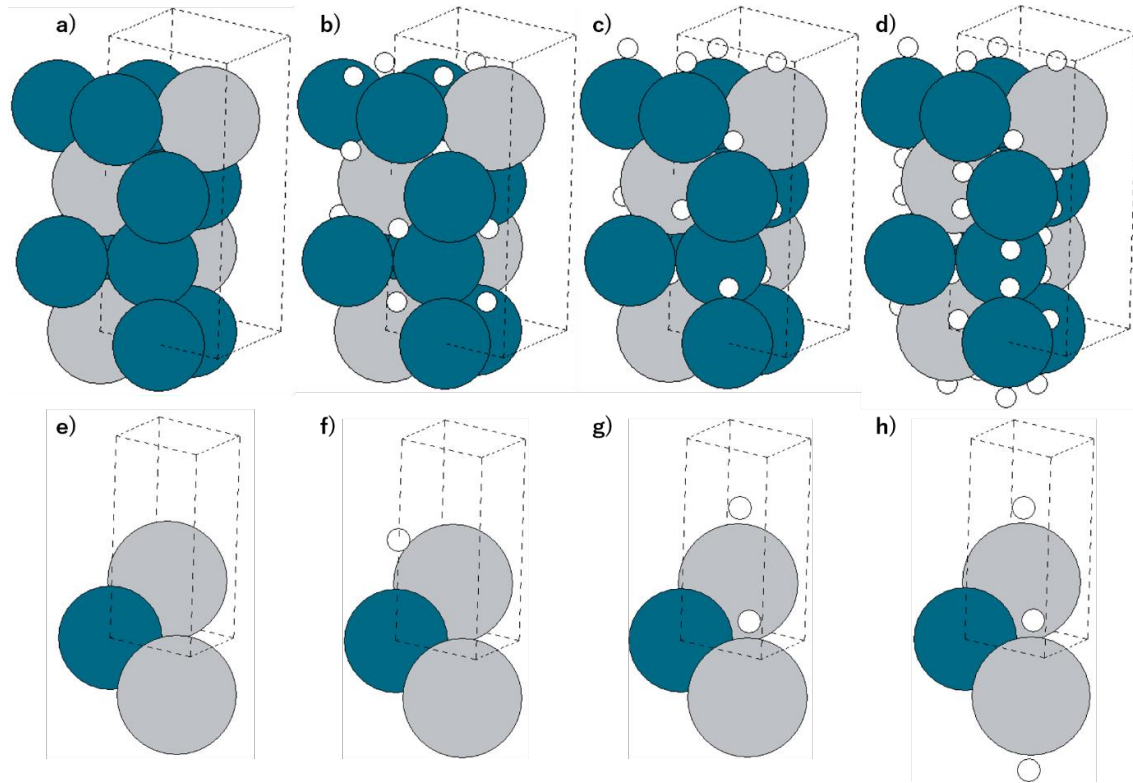


Figure 5: (a) the Pd_3Ti unit cell: 12 Pd atoms and 4 Ti atoms form an HCP structure. (b) with octahedral sites occupied, (c) with wurtzite sites occupied, (d) with tetrahedral sites occupied. (e) the PdTi_2 unit cell: Ti forms an HCP lattice with Pd occupying octahedral sites in alternating layers (f) with other octahedral site occupied, (g) with wurtzite sites occupied, (h) with tetrahedral sites occupied.

ii. FCC Pd-Ti Solid Solution measurements

When loaded with hydrogen, both PdH_{1-x} and TiH_{2-x} exhibit FCC sublattices; it is a reasonable hypothesis that a mixed (Pd,Ti) phase may also show FCC structure under hydrogen loading, especially since cubic phases are more conducive to interstitial occupation. In this case, $\text{Pd}_x\text{Ti}_{1-x}$ would become a solid solution of Pd and Ti with an FCC structure when loaded with hydrogen, and H would occupy some subset of the four octahedral sites and eight

tetrahedral sites within each FCC cell. With this hypothesis in mind, we can imagine creating random FCC matrices of $\text{Pd}_x\text{Ti}_{1-x}$ at various compositions, loading each with hydrogen, and observing the lowest-energy site occupancy in each case. The energy of each solid solution phase can then be compared to that of the loaded binary phases, to see if these structures are indeed physical.

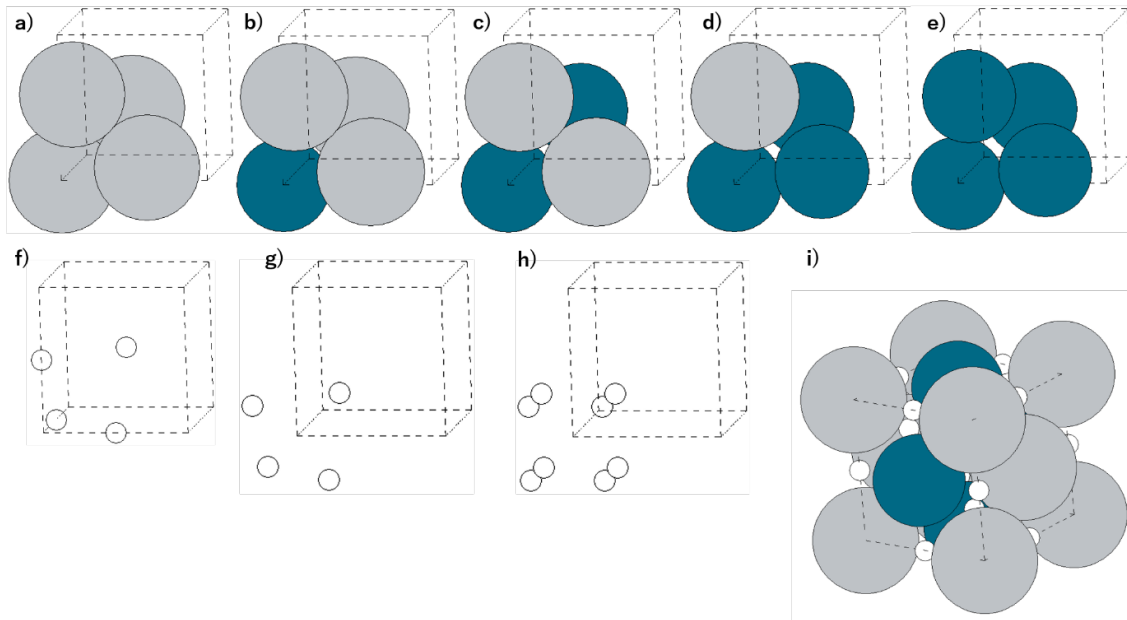


Figure 6: (a-e) the five “solid solution” unit cells. (a) Pd, (b) Pd₃Ti, (c) PdTi, (d) PdTi₃, (e) Ti. (f-h) the three interstitial hydrogen configurations. (f) octahedral sites, (g) zincblende sites, (h) tetrahedral sites. (i) an example cubic unit cell constructed from one of (a-e) and any combination of (f-h).

Although the computational resources available for this thesis made such a study unfeasible over a large supercell, instead our “solid solution” experiments compared the five structures which can be created from a four-atom basis over the cubic unit cell shown in fig.

4: Pd, Pd₃Ti, PdTi, PdTi₃, and Ti. One of these structures, Pd₃Ti, is the on-stoichiometry version of the γ phase. For each of these structures, the energies of six interstitial

occupations were compared: with no hydrogen (M_4), with octahedral or zincblende occupation (M_4H_4), with mixed octahedral-zincblende or tetrahedral occupation (M_4H_8), and with mixed octahedral-tetrahedral occupation (M_4H_{12}). The positions of the metal atoms and interstitial sites are listed in appendix A.

iii. Phase Diagram

The 42 candidate palladium titanium hydride phases examined in this study (six Pd_3Ti phases, six $PdTi_2$ phases, and 30 solid solution phases) can be placed on a palladium-titanium-hydrogen ternary phase diagram (fig. 7). Each point can be given an energy coordinate corresponding to the energy of the phase. The convex hull of these 42 coordinates will then form the ternary phase diagram compiled from these 42 phases, with stable phases at the surface of the hull and unstable phases beneath the surface.

As a result of not including every possible phase in our ternary phase diagram, and especially because of neglecting a pure hydrogen phase (the energy of pure hydrogen was arbitrarily set to zero to produce the convex hull) a phase's stability on the phase diagram does not guarantee that it will be physically realizable. In particular, phases that bound the edges of the diagram are guaranteed to touch the convex hull. However, phases identified as stable are good candidates for further investigation with more a more rigorous computational procedure.

The ternary phase diagram produced here also is for an arbitrary pressure, and will change as the partial pressure of H_2 changes. It is therefore also worthwhile to examine the binary Pd-Ti phase diagrams formed by horizontal slices across the ternary diagram, which captures the stability of phases at fixed hydrogen concentration.

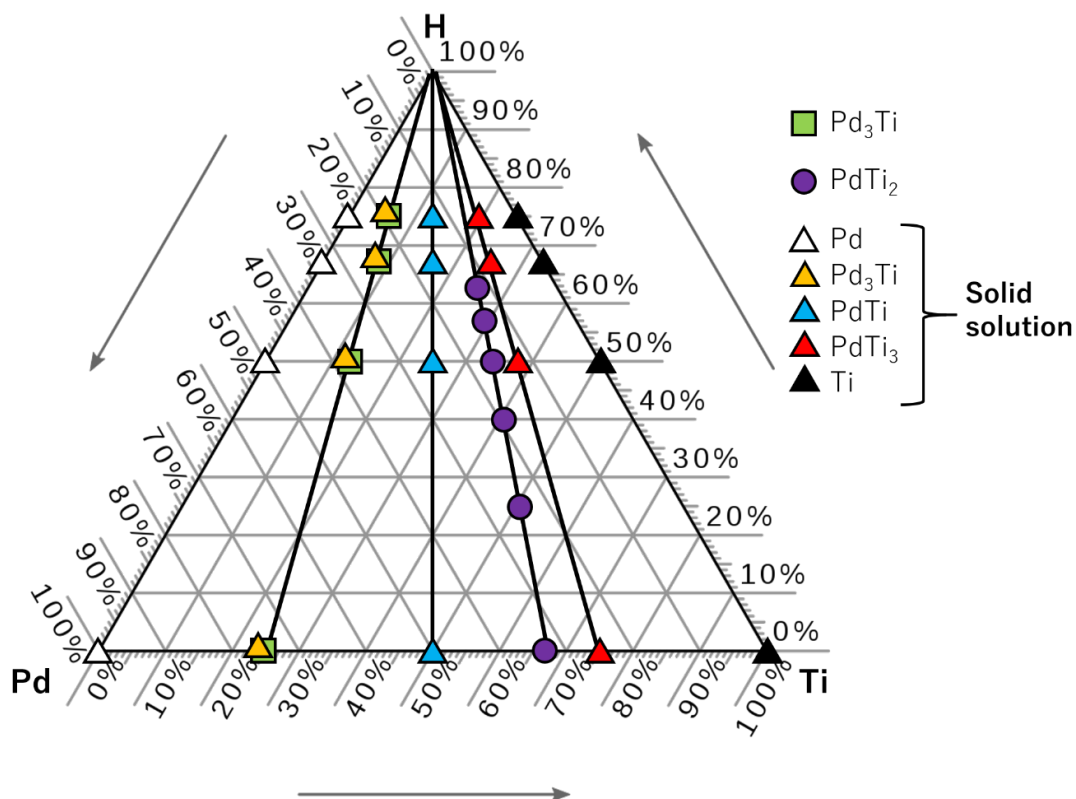


Figure 7: A Pd-Ti-H ternary phase diagram. 42 phases are present, with 26 unique compositions.

Results and Discussion

The energy of each of the 42 structures under study was minimized with respect to lattice parameter. Five lattice constants were chosen near the predicted value and the energy from each was fitted to a parabolic curve. These fits are reproduced in Appendix C.

i. $PdTi_2$

The results of the PdTi₂ calculations are summarized in fig. 8. We see an approximately linear decrease in energy as hydrogen is added to the lattice (fig. 8a). The linear component of this trend is an artifact of the GPAW calculation and is proportional to the number of atoms in the unit cell. This is corrected for in fig. 8b, showing the co-occupancy of octahedral and wurtzite sites to be especially stable. Full tetrahedral occupation, on the other hand, tends to destabilize the lattice.

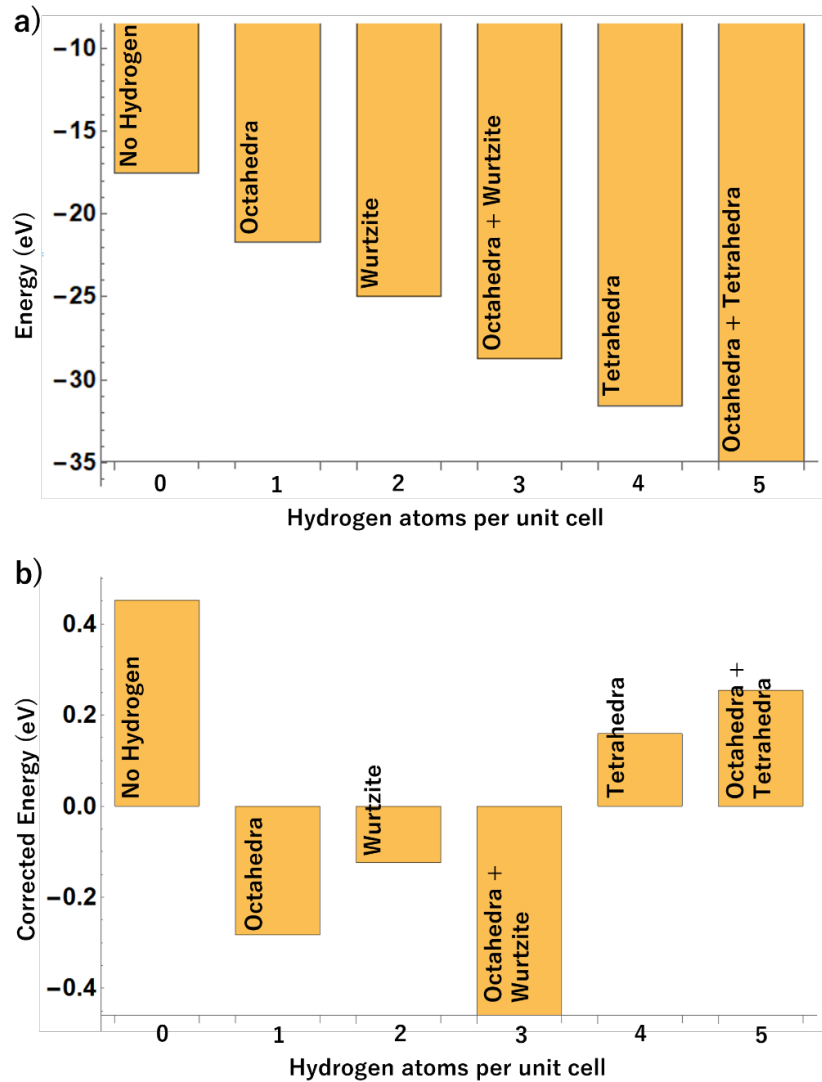


Figure 8: PdTi₂ minimum energies. (a) Uncorrected from the GPAW calculation. A clear linear

trend appears as a result of additional atoms in the unit cell. (b) With the linear trend removed. Octahedral and wurtzite occupation stabilizes the phase, but tetrahedral occupation destabilizes it.

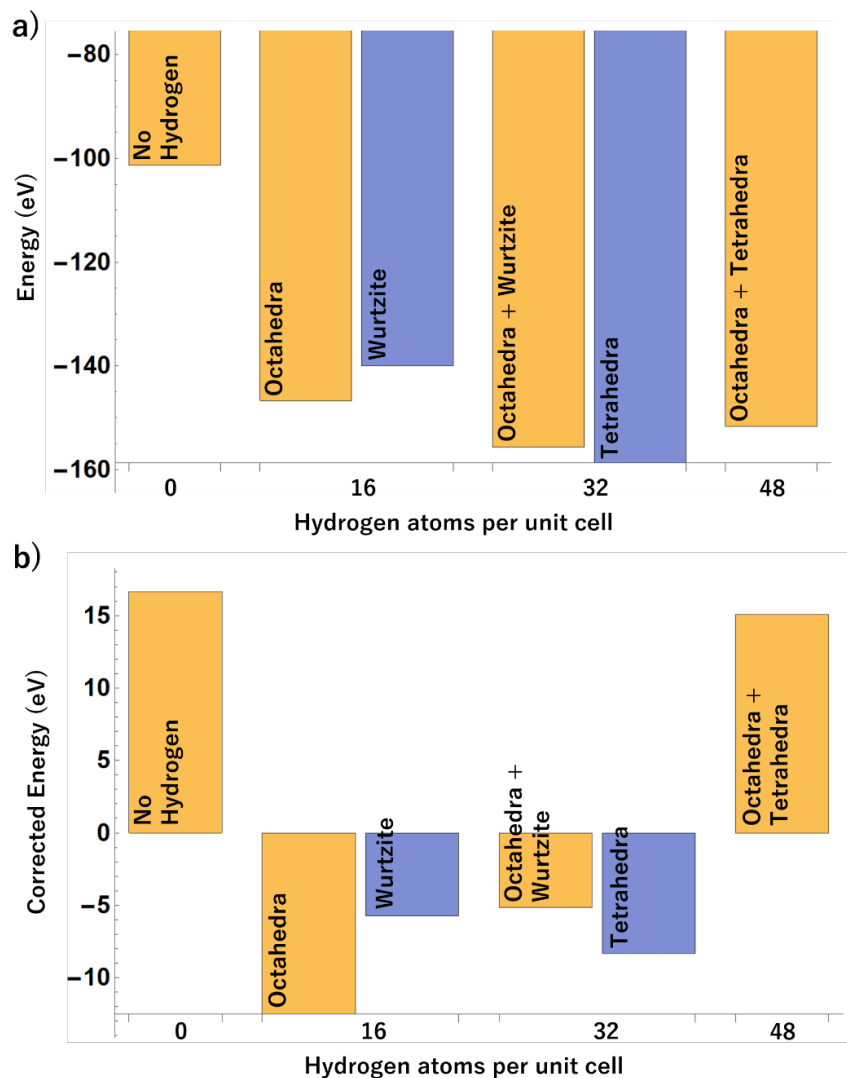


Figure 9: Pd₃Ti minimum energies. (a) uncorrected from the GPAW calculation. (b) With linear trend removed. Octahedral occupation is more stable than wurtzite occupation, and tetrahedral occupation is more stable than mixed octahedral-wurtzite occupation. Mixed octahedral-tetrahedral occupation is very unstable.

ii. Pd₃Ti

The results of the Pd₃Ti computation are summarized in fig. 9. The range of corrected energies in fig. 9b (~25 eV) is much larger than that of fig. 8b (~1eV), partially because the Pd₃Ti unit cell has 16 metal atoms whereas the PdTi₂ unit cell has only three. Even accounting

for the larger unit cell, from fig. 9a one can see that deviations from the expected linear trend in energy are about five times more pronounced in Pd_3Ti , suggesting that interstitial occupancy has a much greater effect on the stability of the structure.

As in PdTi_2 , full occupation of all tetrahedral and octahedral in Pd_3Ti is quite unstable. However, tetrahedral occupation alone isn't as unstable as had been predicted, despite the proximity and lack of screening between tetrahedral sites. It is likely that the lower concentration of Ti atoms in Pd_3Ti makes the hydrogen in the structure less ionic, reducing the hydrogen-hydrogen repulsion and making tetrahedral occupancy less unstable. Still, tetrahedral occupancy in hexagonal structures is extremely rare, and this result requires further investigation.

iii. FCC Pd-Ti Solid Solutions

The results of the solid solution computations are summarized in fig. 10. In each graph, the energy of the unhydrided phase has been set to zero, and the linear trend in data has been removed. As should be expected, the energy of hydrided Ti-rich phases is much lower than that of hydrided Pd-rich phases, because the structure takes on an ionic character.

Contrary to experiment, fig. 10a predicts that PdH will form a zincblende structure rather than rock salt. This implies that the difference in energy between the rock salt and zincblende phases is smaller than the tolerance of our calculation. On the other hand, the fluorite phase of TiH_2 is predicted successfully by a significant margin. Notably, in none of

the cases is full tetrahedral-octahedral occupation the lowest energy phase, and in most it is by far the least stable.

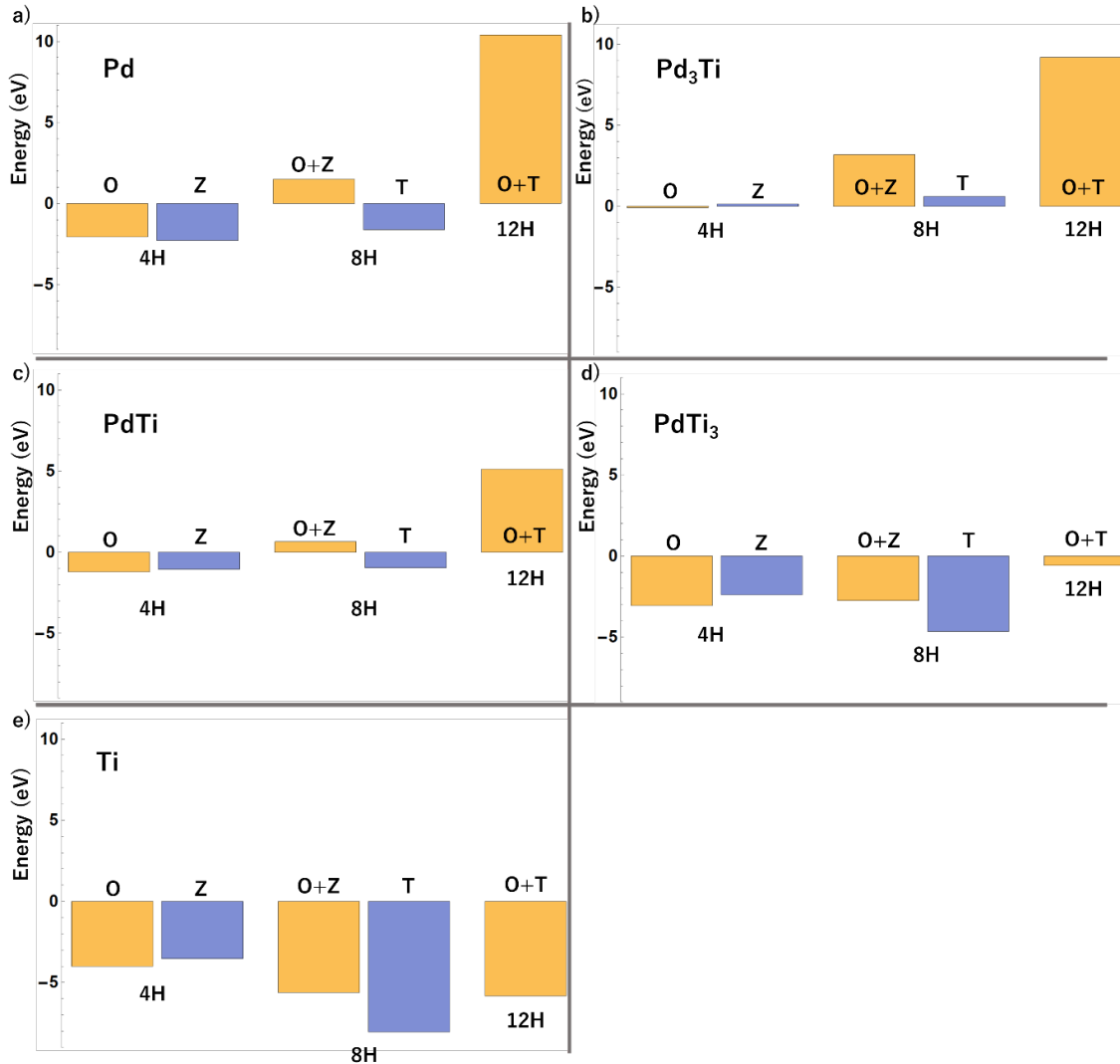


Figure 10: Corrected solid solution minimum energies. (a) Pd, (b) Pd₃Ti, (c) PdTi, (d) PdTi₃, (e) Ti. As [Ti] increases, the high-H phases become more stable, likely due to an increasing ionic character of the interstitial hydrogen.

Fig. 11 compares structures of equal hydrogen concentration for all five solid solution sublattices. MH₂ seems to prefer a rock-salt structure over zincblende for every solid solution except, strangely, pure Pd. MH₄ prefers a fluorite structure over an AgAsMg mixed-

occupation structure for every solid solution, casting doubt on the likelihood of finding a stable instance of mixed occupation experimentally.

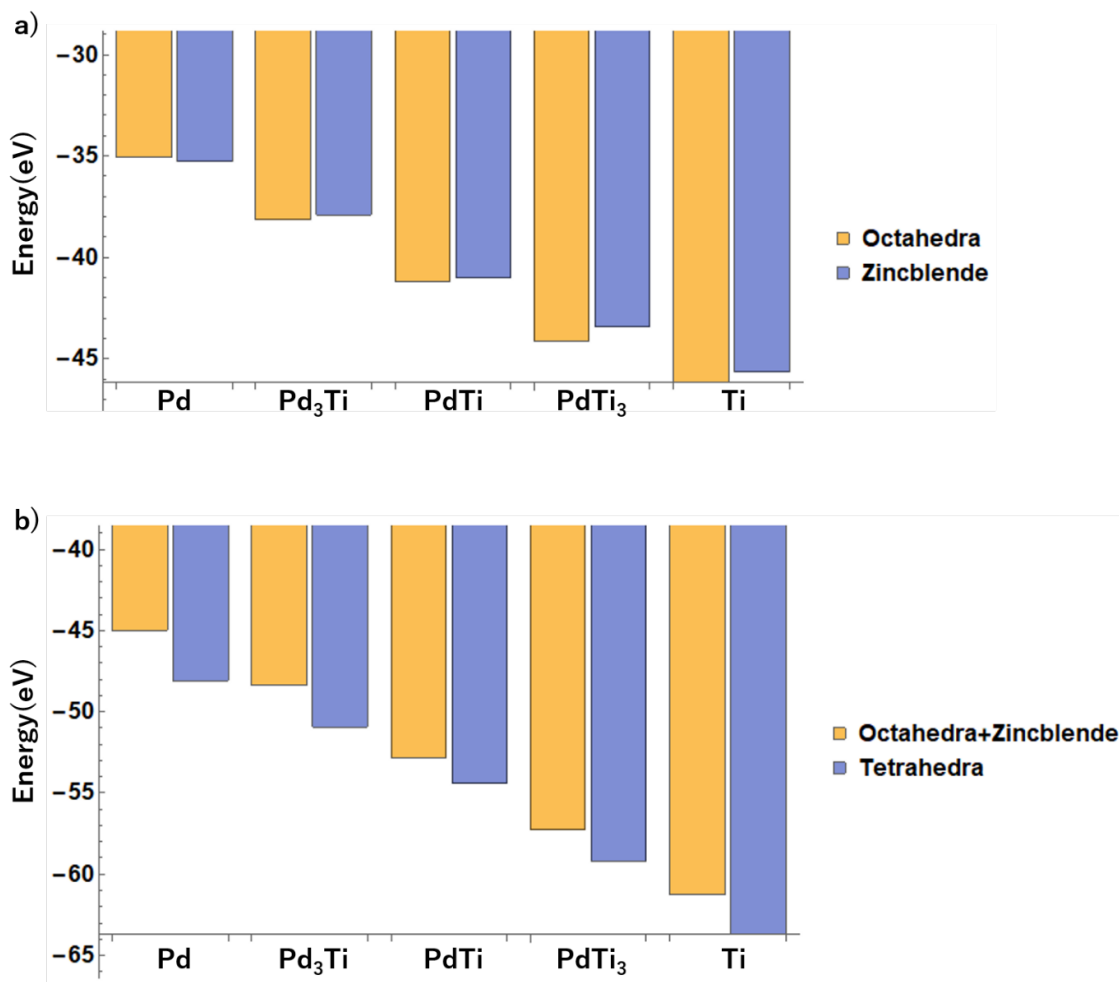


Figure 11: Uncorrected solid solution minimum energies. (a) M₄H₄ structures. Zincblende sites and octahedral sites have comparable stability in Pd, but octahedral sites are more likely to be occupied than zincblende in PdTi₃, PdTi, PdTi₃, and Ti. (b) M₄H₈ structures. Tetrahedral occupation is more stable than mixed octahedral-zincblende occupation in all five lattices.

iv. Phase Diagram

The computational results were compiled to form Pd-Ti binary phase diagrams (fig. 12) and a Pd-Ti-H ternary phase diagram (fig. 13). The convex hull of the uncorrected energies of the phases was used to identify those which would be expressed. Of the

hexagonal structures, only the unhydrided phase of Pd_3Ti was found to be stable – none of the five Pd_3Ti hydrides and none of the PdTi_2 phases was close in energy to the convex hull.

Fig. 12 also shows that mixed octahedral-zincblende or octahedra-wurtzite occupation is less energetically favorable than tetrahedral occupation in every instance.

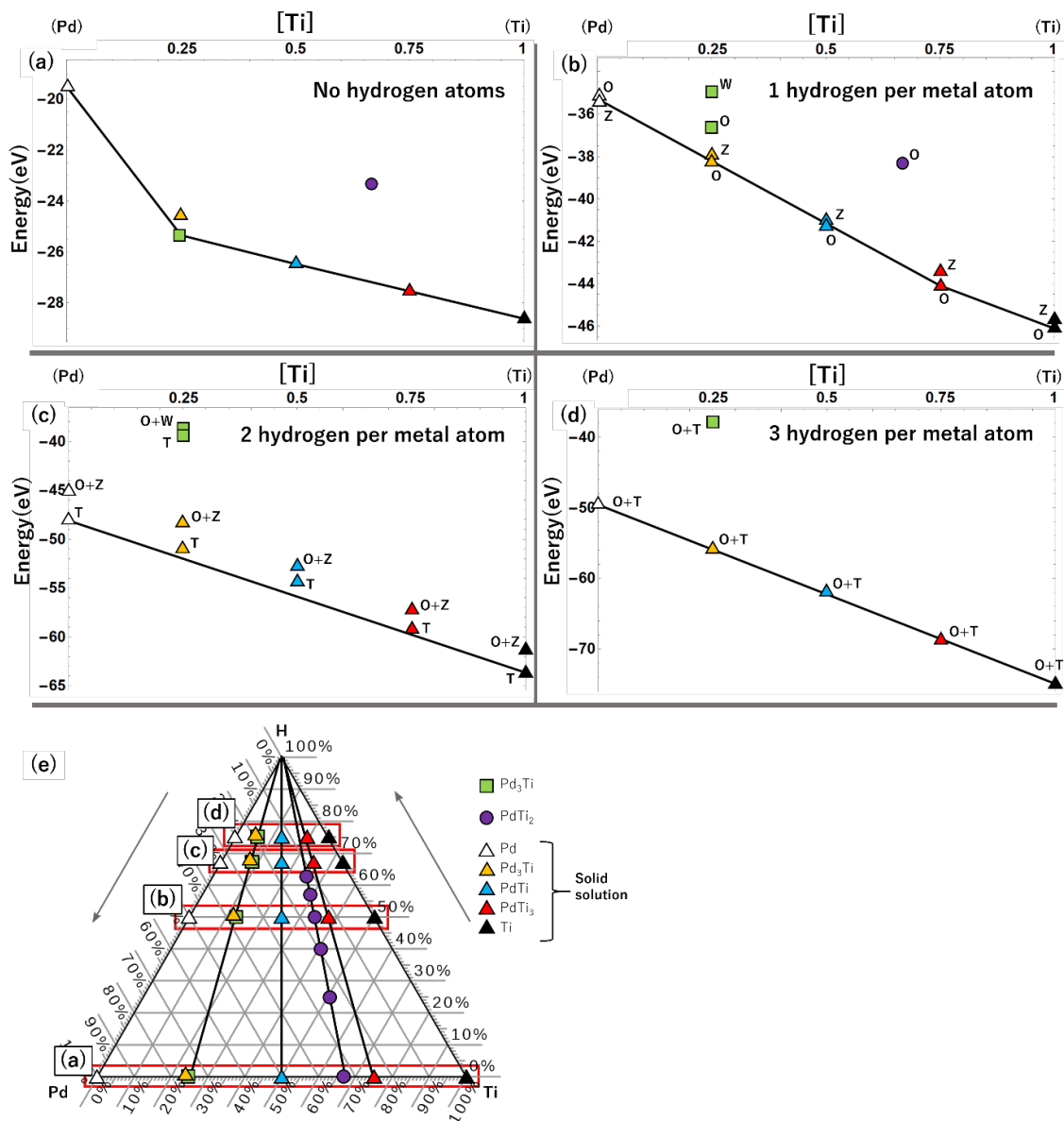


Figure 12: Pd-Ti binary phase diagrams at four different hydrogen concentrations. (a) $\text{Pd}_{1-x}\text{Ti}_x$. (b) $\text{Pd}_{1-x}\text{Ti}_x\text{H}$. (c) $\text{Pd}_{1-x}\text{Ti}_x\text{H}_2$. (d) $\text{Pd}_{1-x}\text{Ti}_x\text{H}_3$. The binary phase diagrams are slices of the ternary Pd-Ti-H phase diagram, and their positions on this ternary phase diagram are shown in (e)

Fig. 13 shows the ternary phase diagram formed by taking the convex hull of the coordinates and energies of all 42 under study. This ternary phase diagram is necessarily incomplete because it lacks a pure hydrogen phase, but it nonetheless can provide some insight. As expected from the binary phase diagrams, none of the hydride hexagonal phases appear. A few interesting phases do appear to be stable, however: fluorite-prototype PdH and Li_3Bi -prototypes TiH_3 , PdH_3 , and $\text{PdTi}_3\text{H}_{12}$. In fact, all five Li_3Bi prototypes lie nearly perfectly along the edge of the convex hull. Unfortunately, most or all of these phases are likely artifacts of the incomplete ternary phase diagram, and the convex hull pinning on the bounding region of the diagram. Nonetheless, these Li_3Bi structures might be interesting to examine in more detail.

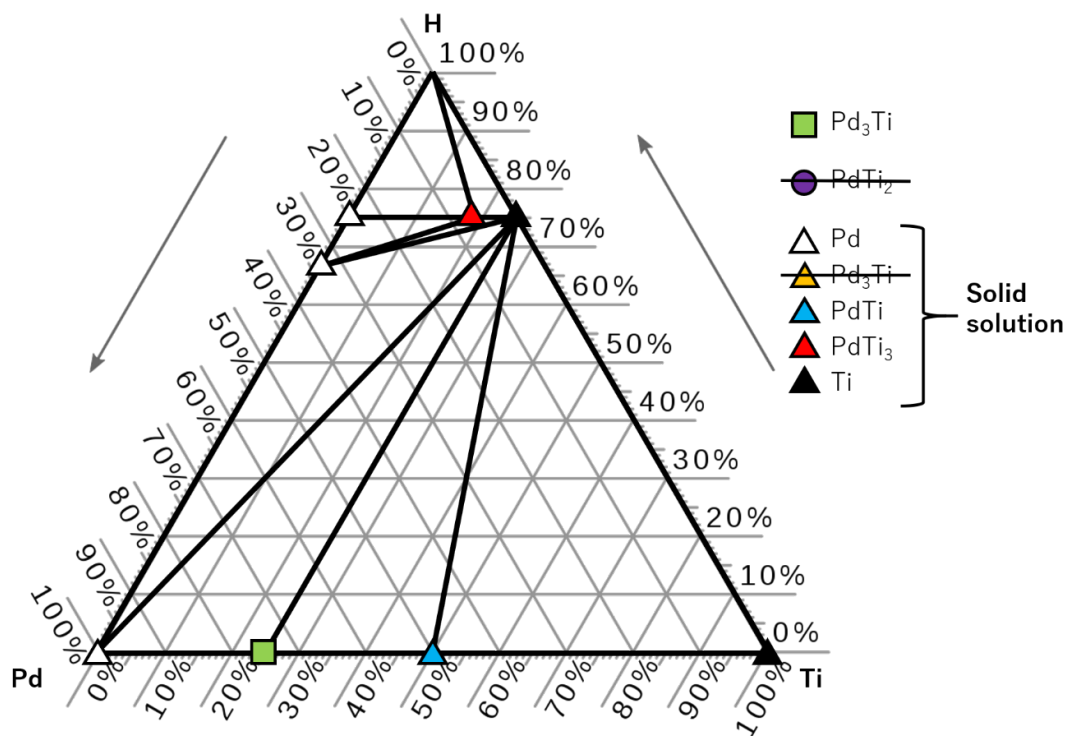


Figure 13: The Pd-Ti-H ternary phase diagram.

Conclusion

This study used density functional theory tools to search for stable instances of mixed tetrahedral-octahedral interstitial occupation in hydrided Pd-Ti lattices. A comparison of the energies of 42 metal hydride phases built from three types of Pd-Ti sublattice suggested that cubic structures more readily accept interstitial hydrogen than hexagonal structures, but that every structure prefers to fill all tetrahedral sites before beginning to fill octahedral sites. The ternary phase diagram constructed from the 42 phases is biased towards phases with high hydrogen loading, but nonetheless identifies $\text{Pd}_{1-x}\text{Ti}_x\text{H}_3$ as one candidate system to search for mixed octahedral-tetrahedral site occupation. The hexagonal Pd_3TiH_8 phase with full tetrahedral occupation was also found to be more stable than expected, though not stable enough to appear on the phase diagram. Future work can examine TiH_3 and Pd_3TiH_8 more rigorously, first from a computational standpoint and then experimentally, to confirm or refute the stability of the phase.

Works Cited

- [1] L. Gillespie and L Galstaun, “The Palladium-Hydrogen Equilibrium and New Palladium Hydrides”. J. Am. Chem. Soc. (1936).
- [2] *Phase Diagrams*, ASM International
- [3] P. Hohenberg and W. Kohn, “Inhomogeneous Electron Gas”, Phys. Rev. (1964).
- [4] W. Kohn and L. Sham, “Self-Consistent Equations Including Exchange and Correlation Effects”, Phys. Rev. (1965).
- [5] D. Sholl and J. Steckel, “Density Functional Theory: A Practical Introduction”, John Wiley & Sons, Inc. (2009)
- [6] A. Larsen et al., “The atomic simulation environment—a Python library for working with atoms”, J. Phys.: Condens. Matter (2017).
- [7] C. Rostgaard, “The Projector Augmented-wave Method”, ArXiv.org (2009)
- [8] J. Enkovaara, C. Rostgaard, J. Mortensen et al., “Electronic structure calculations with GPAW: a real-space implementation of the projector augmented-wave method”, J. Phys.: Condens. Matter (2010)
- [9] H. Okamoto, “Pd-Ti (Palladium-Titanium)”, J. Phase Equil. Diff. (2013).
- [10] M. Mehl et al., “The AFLOW Library of Crystallographic Prototypes: Part 1”, Comp. Mat. Sci. (2017).

Appendix A: Atomic Positions and Unit Cells

i. PdTi₂

Lattice Vectors	$a_1 = [a/2, -\sqrt{3}a/2, 0]$ $a_2 = [a/2, \sqrt{3}a/2, 0]$ $a_3 = [0, 0, c]$		
	$c=1.633a$, $z=0.252$		
Metal atoms	Pd: $[0, 0, 0]$ Ti: $[a/2, a/(\sqrt{3} \cdot 2), c \cdot z]$ $[a/2, -a/(\sqrt{3} \cdot 2), -c \cdot z]$		
Interstitial sites	Octahedra	Wurtzite	Tetrahedra
	$[0, 0, c/2]$	$[a/2, a/(\sqrt{3} \cdot 2), (3c - 2cz)/4]$ $[a/2, -a/(\sqrt{3} \cdot 2), c \cdot z/2]$	$[a/2, a/(\sqrt{3} \cdot 2), (3c - 2cz)/4]$ $[a/2, a/(\sqrt{3} \cdot 2), -c \cdot z/2]$ $[a/2, -a/(\sqrt{3} \cdot 2), c \cdot z/2]$ $[a/2, -a/(\sqrt{3} \cdot 2), (-3c + 2cz)/4]$

ii. Pd₃Ti

Lattice Vectors	$a_1 = [a/2, -\sqrt{3}a/2, 0]$ $a_2 = [a/2, \sqrt{3}a/2, 0]$ $a_3 = [0, 0, c]$		
	$c=1.633a$, $x_4= -1/6$		
Metal atoms	Pd: $[a/4, -\sqrt{3}a/4, 0]$ $[a/4, \sqrt{3}a/4, 0]$ $[a/2, 0, 0]$ $[a/4, \sqrt{3}a/4, c/2]$ $[a/4, -\sqrt{3}a/4, c/2]$ $[a/2, 0, c/2]$ $[3a \cdot x_4/2, \sqrt{3} \cdot x_4 \cdot a/2, c/4]$ $[-3a \cdot x_4/2, \sqrt{3} \cdot x_4 \cdot a/2, c/4]$ Ti: $[0, -\sqrt{3} \cdot x_4 \cdot a, c/4]$ $[-3 \cdot x_4 \cdot a/2, -\sqrt{3} \cdot x_4 \cdot a/2, 3 \cdot c/4]$ $[3 \cdot x_4 \cdot a/2, -\sqrt{3} \cdot x_4 \cdot a/2, 3 \cdot c/4]$ $[0, \sqrt{3} \cdot x_4 \cdot a, 3 \cdot c/4]$ Ti: $[0, 0, 0]$ $[0, 0, c/2]$ $[a/2, a/(2 \cdot \sqrt{3}), c/4]$ $[a/2, -a/(2 \cdot \sqrt{3}), 3 \cdot c/4]$		

	Octahedra	Wurtzite	Tetrahedra
Interstitial sites	$[a/2, -(a/(2*\sqrt{3})), c/8]$	$[0, 0, (11*c)/16]$	$[0, 0, (11*c)/16]$
	$[a/2, -(a/(2*\sqrt{3})), (3*c)/8]$	$[0, 0, (3*c)/16]$	$[0, 0, (5*c)/16]$
	$[-((3*a*x4)/2), -(1/2)*\sqrt{3}*a*x4, c/8]$	$[a/4, -((\sqrt{3}*a)/4), (11*c)/16]$	$[0, 0, (3*c)/16]$
	$[-((3*a*x4)/2), -(1/2)*\sqrt{3}*a*x4 (3*c)/8]$	$[a/4, -((\sqrt{3}*a)/4), (3*c)/16]$	$[0, 0, -(3*c)/16]$
	$[(3*a*x4)/2, -(1/2)*\sqrt{3}*a*x4, c/8]$	$[a/4, (\sqrt{3}*a)/4, (11*c)/16]$	$[a/4, -((\sqrt{3}*a)/4), (11*c)/16]$
	$[(3*a*x4)/2, -(1/2)*\sqrt{3}*a*x4 (3*c)/8]$	$[a/4, (\sqrt{3}*a)/4, (3*c)/16]$	$[a/4, -((\sqrt{3}*a)/4), (5*c)/16]$
	$[0, \sqrt{3}*a*x4, c/8]$	$[a/2, 0, (11*c)/16]$	$[a/4, -((\sqrt{3}*a)/4), (3*c)/16]$
	$[0, \sqrt{3}*a*x4, (3*c)/8]$	$[a/2, 0, (3*c)/16]$	$[a/4, -((\sqrt{3}*a)/4), -(3*c)/16]$
	$[a/2, a/(2*\sqrt{3}), (7*c)/8]$	$[a/2, -(a/(2*\sqrt{3})), (15*c)/16]$	$[a/4, (\sqrt{3}*a)/4, (11*c)/16]$
	$[a/2, a/(2*\sqrt{3}), (5*c)/8]$	$[a/2, -(a/(2*\sqrt{3})), (7*c)/16]$	$[a/4, (\sqrt{3}*a)/4, (5*c)/16]$
	$[(3*a*x4)/2, 1/2*\sqrt{3}*a*x4, (7*c)/8]$	$[-((3*a*x4)/2), -(1/2)*\sqrt{3}*a*x4, (15*c)/16]$	$[a/4, (\sqrt{3}*a)/4, (3*c)/16]$
	$[(3*a*x4)/2, 1/2*\sqrt{3}*a*x4, (5*c)/8]$	$[-((3*a*x4)/2), -(1/2)*\sqrt{3}*a*x4, (7*c)/16]$	$[a/2, 0, (11*c)/16]$
	$[-((3*a*x4)/2), 1/2*\sqrt{3}*a*x4, (7*c)/8]$	$[(3*a*x4)/2, -(1/2)*\sqrt{3}*a*x4 (15*c)/16]$	$[a/2, 0, (5*c)/16]$
	$[-((3*a*x4)/2), 1/2*\sqrt{3}*a*x4, (5*c)/8]$	$[(3*a*x4)/2, -(1/2)*\sqrt{3}*a*x4 (15*c)/16]$	$[a/2, 0, (3*c)/16]$
	$[0, -\sqrt{3}*a*x4, (7*c)/8]$	$[0, \sqrt{3}*a*x4, (15*c)/16]$	$[a/2, 0, -(3*c)/16]$
	$[0, -\sqrt{3}*a*x4, (5*c)/8]$	$[0, \sqrt{3}*a*x4, (7*c)/16]$	$[a/2, -(a/(2*\sqrt{3})), (15*c)/16]$
			$[a/2, -(a/(2*\sqrt{3})), (9*c)/16]$
			$[a/2, -(a/(2*\sqrt{3})), (7*c)/16]$
			$[a/2, -(a/(2*\sqrt{3})), c/16]$
			$[-((3*a*x4)/2), -(1/2)*\sqrt{3}*a*x4, (15*c)/16]$
		$[-((3*a*x4)/2), -(1/2)*\sqrt{3}*a*x4, (9*c)/16]$	
		$[-((3*a*x4)/2), -(1/2)*\sqrt{3}*a*x4, c/16]$	
		$[(3*a*x4)/2, -(1/2)*\sqrt{3}*a*x4, (15*c)/16]$	
		$[(3*a*x4)/2, -(1/2)*\sqrt{3}*a*x4, (9*c)/16]$	
		$[(3*a*x4)/2, -(1/2)*\sqrt{3}*a*x4, (7*c)/16]$	
		$[(3*a*x4)/2, -(1/2)*\sqrt{3}*a*x4, c/16]$	

			$[0, \sqrt{3}a^2x^4, (15c)/16]$ $[0, \sqrt{3}a^2x^4, (9c)/16]$ $[0, \sqrt{3}a^2x^4, (7c)/16]$ $[0, \sqrt{3}a^2x^4, c/16]$
--	--	--	--

iii. Solid Solution

Lattice Vectors	$a_1 = [a, 0, 0]$ $a_2 = [0, a, 0]$ $a_3 = [0, 0, a]$		
Metal atoms	$[0, 0, 0]$ $[a/2, a/2, 0]$ $[a/2, 0, a/2]$ $[0, a/2, a/2]$		
Interstitial sites	Octahedra	Zincblende	Tetrahedra
	$[a/2, 0, 0]$ $[0, a/2, 0]$ $[0, 0, a/2]$ $[a/2, a/2, a/2]$	$[a/4, a/4, a/4]$ $[a/4, -a/4, -a/4]$ $[-a/4, a/4, -a/4]$ $[-a/4, -a/4, a/4]$	$[a/4, a/4, a/4]$ $[a/4, a/4, -a/4]$ $[a/4, -a/4, a/4]$ $[a/4, -a/4, -a/4]$ $[-a/4, a/4, a/4]$ $[-a/4, a/4, -a/4]$ $[-a/4, -a/4, a/4]$ $[-a/4, -a/4, -a/4]$

Appendix B: ASE Code

i. PdTi₂

```

from ase import Atoms
from gpaw import GPAW, PW

k = 6 #num k-points
calc = GPAW(mode=PW(300),kpts=(k, k, k))

a=3
c=1.633*a
z=.252

unitcell=[[a/2, -1.73205*a/2,0],[a/2,1.73205*a/2,0],[0,0,c]]

pos=[[0,0,0],[a/2,a/(1.73205*2),c*z],[a/2,-a/(1.73205*2),-c*z]]

tetrahedra=Atoms('H4',[[a/2,a/(1.73205*2),(3*c-2*c*z)/4],[a/2,a/(1.73205*2),-c*z/2],[a/2,-a/(1.73205*2),c*z/2],[a/2,-a/(1.73205*2),(-3*c+2*c*z)/4]],cell=unitcell,cbc=True)

wurtzite=Atoms('H2',[[a/2,a/(1.73205*2),(3*c-2*c*z)/4],[a/2,-a/(1.73205*2),c*z/2]],cell=unitcell,cbc=True)

octahedra=Atoms('H',[[0,0,c/2]],cell=unitcell,cbc=True)

energies=[]
for i in range(6):
    pdti2=Atoms('PdTi2',positions=pos,cell=unitcell,cbc=True,calculator=calc)
    if i in range(3):
        pdti2.extend(octahedra)
    if i in [0,3]:
        pdti2.extend(wurtzite)
    if i in [1,4]:
        pdti2.extend(tetrahedra)

    for j in range(5):
        x=.9+.05*j
        unitcellx=[[a*x/2, -1.73205*a*x/2,0],[a*x/2,1.73205*a*x/2,0],[0,0,c*x]]

```

```

pdti2.set_cell(unitcellx, scale_atoms=True) #scale unit cell
energy=pdti2.get_potential_energy() #find energy
energies.append(energy) #write energy
energy=[]
##### END OF FOR LOOP #####
print(energies)

```

ii. Pd₃Ti

```

from ase import Atoms
from gpaw import GPAW, PW

k = 6 #num k-points.
calc = GPAW(mode=PW(300),kpts=(k, k, k)) # output file

a=5
c=1.633*a
x4=-1/6

unitcell=[[a/2,-1*1.73205*a/2,0],[a/2,1.73205*a/2,0],[0,0,c]]

tetrahedra=Atoms('H32',positions=[[0,0,(11*c)/16],[0,0,(5*c)/16],[0,0,(3*c)/16],[0,0,-
1*((3*c)/16)],[a/4,-1*((1.73205*a)/4),(11*c)/16],[a/4,-1*((1.73205*a)/4),(5*c)/16],[a/4,-
1*((1.73205*a)/4),(3*c)/16],[a/4,-1*((1.73205*a)/4),-
1*((3*c)/16)],[a/4,(1.73205*a)/4,(11*c)/16],[a/4,(1.73205*a)/4,(5*c)/16],[a/4,(1.73205*a)/4,(3*c)/16],
[a/4,(1.73205*a)/4,-1*((3*c)/16)],[a/2,0,(11*c)/16],[a/2,0,(5*c)/16],[a/2,0,(3*c)/16],[a/2,0,-
1*((3*c)/16)],[a/2,-1*(a/(2*1.73205)),(15*c)/16],[a/2,-1*(a/(2*1.73205)),(9*c)/16],[a/2,-
1*(a/(2*1.73205)),(7*c)/16],[a/2,-1*(a/(2*1.73205)),c/16],[-1*((3*a*x4)/2),-
1*(1/2)*1.73205*a*x4,(15*c)/16],[-1*((3*a*x4)/2),-1*(1/2)*1.73205*a*x4,(9*c)/16],[-1*((3*a*x4)/2),-
1*(1/2)*1.73205*a*x4,(7*c)/16],[-1*((3*a*x4)/2),-1*(1/2)*1.73205*a*x4,c/16],[((3*a*x4)/2),-
1*(1/2)*1.73205*a*x4,(15*c)/16],[((3*a*x4)/2),-1*(1/2)*1.73205*a*x4,(9*c)/16],[((3*a*x4)/2),-
1*(1/2)*1.73205*a*x4,(7*c)/16],[((3*a*x4)/2),-
1*(1/2)*1.73205*a*x4,c/16],[0,1.73205*a*x4,(15*c)/16],[0,1.73205*a*x4,(9*c)/16],[0,1.73205*a*x4,(7*c)/
16],[0,1.73205*a*x4,c/16]],cell=unitcell,abc=True)

wurtzite=Atoms('H16',positions=[[0,0,(11*c)/16],[0,0,(3*c)/16],[a/4,-((1.73205*a)/4),(11*c)/16],[a/4,-
((1.73205*a)/4),(3*c)/16],[a/4,(1.73205*a)/4,(11*c)/16],[a/4,(1.73205*a)/4,(3*c)/16],[a/2,0,(11*c)/16]
,[a/2,0,(3*c)/16],[a/2,-(a/(2*1.73205)),(15*c)/16],[a/2,-(a/(2*1.73205)),(7*c)/16],[-((3*a*x4)/2),-
(1/2)*1.73205*a*x4,(15*c)/16],[-((3*a*x4)/2),-(1/2)*1.73205*a*x4,(7*c)/16],[((3*a*x4)/2),-
(1/2)*1.73205*a*x4,(15*c)/16],[((3*a*x4)/2),-

```

```
(1/2)*1.73205*a*x4,(7*c)/16],[0,1.73205*a*x4,(15*c)/16],[0,1.73205*a*x4,(7*c)/16]],cell=unitcell,abc=True)
```

```
octahedra=Atoms('H16',positions=[[a/2,-(a/(2*1.73205)),c/8],[a/2,-(a/(2*1.73205)),(3*c)/8],[-(3*a*x4)/2,-(1/2)*1.73205*a*x4,c/8],[-(3*a*x4)/2,-(1/2)*1.73205*a*x4,(3*c)/8],[(3*a*x4)/2,-(1/2)*1.73205*a*x4,c/8],[(3*a*x4)/2,-(1/2)*1.73205*a*x4,(3*c)/8],[0,1.73205*a*x4,c/8],[0,1.73205*a*x4,(3*c)/8],[a/2,a/(2*1.73205),(7*c)/8],[a/2,a/(2*1.73205),(5*c)/8],[(3*a*x4)/2,1/2*1.73205*a*x4,(7*c)/8],[(3*a*x4)/2,1/2*1.73205*a*x4,(5*c)/8],[-(3*a*x4)/2,1/2*1.73205*a*x4,(7*c)/8],[-(3*a*x4)/2,1/2*1.73205*a*x4,(5*c)/8],[0,-1.73205*a*x4,(7*c)/8],[0,-1.73205*a*x4,(5*c)/8]],cell=unitcell,abc=True)
```

```
energies=[]
```

```
for i in range(6):
```

```
    pd3ti=Atoms('Ti4Pd12',positions=[[0,0,0],[0,0,c/2],[a/2,a/(2*1.73205),c/4],[a/2,-a/(2*1.73205),3*c/4],[a/4,-1*1.73205*a/4,0],[a/4,1.73205*a/4,0],[a/2,0,0],[a/4,-1*1.73205*a/4,c/2],[a/4,1.73205*a/4,c/2],[a/2,0,c/2],[3*a*x4/2,1.73205*x4*a/2,c/4],[3*a*x4/2,1.73205*x4*a/2,c/4],[0,-1*1.73205*x4*a,c/4],[-3*x4*a/2,-1*1.73205*x4*a/2,3*c/4],[3*x4*a/2,-1*1.73205*x4*a/2,3*c/4],[0,1.73205*x4*a,3*c/4]],cell=unitcell,abc=True,calculator=calc)
```

```
    if i in range(3):
```

```
        pd3ti.extend(octahedra)
```

```
    if i in [0,3]:
```

```
        pd3ti.extend(wurtzite)
```

```
    if i in [1,4]:
```

```
        pd3ti.extend(tetrahedra)
```

```
for j in range(5):
```

```
    x=.9+.05*j
```

```
    unitcellx=[[x*a/2,-1.73205*x*a/2,0],[x*a/2,1.73205*x*a/2,0],[0,0,c*x]]
```

```
    pd3ti.set_cell(unitcellx, scale_atoms=True) #scale unit cell
```

```
    energy=pd3ti.get_potential_energy() #find energy
```

```
    energies.append(energy) #write energy
```

```
    energy=[]
```

```
##### END OF FOR LOOP #####
```

```
print(energies)
```

iii. Solid Solution

```
from ase import Atoms
```

```
from gpaw import GPAW, PW
```

```

k = 6 #num k-points.
calc = GPAW(mode=PW(300),kpts=(k, k, k)) # output file

a=4
cube=[[a,0,0],[0,a,0],[0,0,a]]

tetrahedra=Atoms('H8',[[a/4,a/4,a/4],[a/4,a/4,-a/4],[a/4,-a/4,a/4],[a/4,-a/4,-a/4],[-a/4,a/4,a/4],[-a/4,a/4,-a/4],[-a/4,-a/4,a/4],[-a/4,-a/4,-a/4]],cell=cube,abc=True)

zinblend=Atoms('H4',[[a/4,a/4,a/4],[a/4,-a/4,-a/4],[-a/4,a/4,-a/4],[-a/4,-a/4,a/4]],cell=cube,abc=True)

octahedra=Atoms('H4',[[a/2,0,0],[0,a/2,0],[0,0,a/2],[a/2,a/2,a/2]],cell=cube,abc=True)

struct=Atoms('Ti4',positions=[[0,0,0],[a/2,a/2,0],[a/2,0,a/2],[0,a/2,a/2]],cell=cube,abc=True,calculator=calc)

energies=[]

for i in range(30): #compare the stability of 30 structures
    #build struct
    if i in range(15):
        struct.extend(octahedra) #1/2 w octahedral sites filled

    if i in range(0,5) or i in range(15,20): #1/3 w zinblend sites filled
        struct.extend(zinblend)

    if i in range(5,10) or i in range(20,25): #1/3 w tetrahedral sites filled
        struct.extend(tetrahedra)

    if i in [0,5,10,15,20,25]: # #1/5 with 0 pd, 1/5 w 1 pd
        struct.symbols[0]='Pd'

    if i in [1,6,11,16,21,26]: #1/5 with 2 pd
        struct.symbols[0]='Pd'
        struct.symbols[1]='Pd'

    if i in [2,7,12,17,22,27]: #1/5 with 3 pd
        struct.symbols[0]='Pd'

```

```

struct.symbols[1]='Pd'
struct.symbols[2]='Pd'

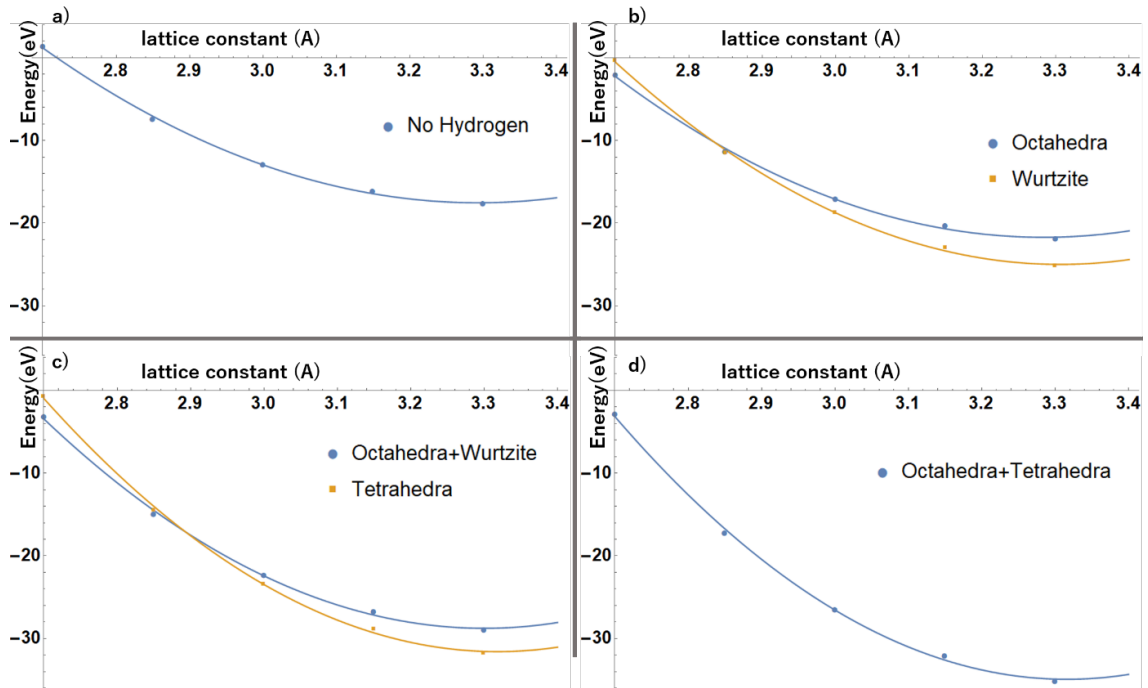
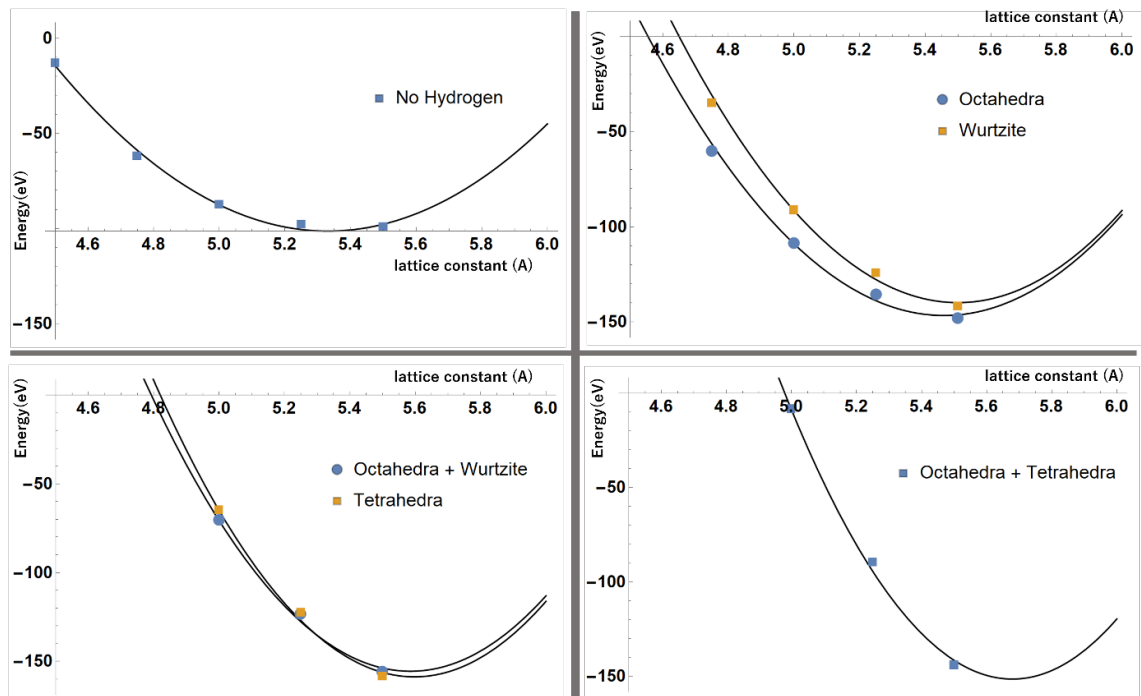
if i in [3,8,13,18,23,28]: #1/5 with 4 pd
    struct.symbols[0]='Pd'
    struct.symbols[1]='Pd'
    struct.symbols[2]='Pd'
    struct.symbols[3]='Pd'

#####
for x in range(5):
    y=.9+.05*x
    cubey=[[a*y,0,0],[0,a*y,0],[0,0,a*y]]
    struct.set_cell(cubey, scale_atoms=True) #scale unit cell
    energy=struct.get_potential_energy() #find energy
    energies.append(energy)
    energy=[]

#####
#reset for the next loop
atoms=4
struct=Atoms('Ti4',positions=[[0,0,0],[a/2,a/2,0],[a/2,0,a/2],[0,a/2,a/2]],cell=cube,dbc=True,calculator=calc) #reset the skeleton structure for the next iteration
##### END OF FOR LOOP #####
print (energies)

```

Appendix C: Calculation Results

i. PdTi₂ii. Pd₃Ti

iii. Solid Solution

